Biosensors and Bioelectronics 130 (2019) 269–275

Contents lists available at ScienceDirect

Biosensors and Bioelectronics

journal homepage: www.elsevier.com/locate/bios

Photoelectrochemical platform for MicroRNA let-7a detection based on graphdiyne loaded with AuNPs modified electrode coupled with alkaline phosphatase

Yanxin Li[a], Xiaohua Li[b], Yuchan Meng[a], Xu Hun[a,*]

[a] Key Laboratory of Optic-electric Sensing and Analytical Chemistry for Life Science, MOE; Shandong Key Laboratory of Biochemical Analysis; Key Laboratory of Analytical Chemistry for Life Science in Universities of Shandong; State Key Laboratory Base of Eco-chemical Engineering; Key Laboratory of Rubber-Plastics of Ministry of Education/Shandong Provincial Key Laboratory of Rubber Plastics; College of Chemistry and Molecular Engineering, Qingdao University of Science and Technology, Qingdao 266042, China

[b] School of Chemistry and Environmental Engineering, Shanxi Datong University, Shanxi 037009, China

ARTICLE INFO

Keywords:
Photoelectrochemical
Graphdiyne
Photoactive Material
microRNA
AuNPs
Alkaline Phosphatase

ABSTRACT

In this work, a photoactive material, Graphdiyne (GDY) loaded with AuNPs (AuNPs-GDY), was successfully synthesized. The fabricated material made use of the natural band-gap structure of GDY, which could produce hole-electron pairs and the plasmon resonance effect of AuNPs to obtain a high photoelectrochemical (PEC) response. AuNPs-GDY PEC response changed with the mass ratio of GDY to tetrachloroauric acid. When the mass ratio of GDY to tetrachloroauric acid was 1:2.5, AuNPs-GDY exhibited the best PEC performance. Thus, the best one was selected as the photoactive material to establish a PEC biosensor for microRNA detection. The PEC biosensor used the alkaline phosphatases as catalyzer to generate ascorbic acid in situ, which provided a low background signal and a high PEC response. The cancer marker, MicroRNA let-7a, was chosen as a target model. Under optimal condition, potential 300 mV and pH 8.0, the PEC biosensor had a detection limit of 3.3×10^{-19} M and a good linearity with microRNA let-7a concentration ranged from 1.0×10^{-18} M to 1.0×10^{-10} M. This PEC biosensor opened a promising platform using GDY to fabricate analytical method and detect microRNA at ultralow levels for diagnoses.

1. Introduction

PEC was an emerged and burgeoning detection method. Under the excitation of light, the electrons in the valence band (VB) of photoactive materials transited to the conduction band (CB). The photoinduced electron transferred between the interfaces of electrode and solution to generate photocurrent (Yang et al., 2018). Due to its high sensitivity and low cost (Zhao et al., 2014), PEC detection methods were widely used (Fan et al., 2018a, 2018b; Li et al., 2018b; Peng et al., 2018). Firstly, finding new effective optical sensing materials was a vital task to fabricate PEC biosensor. In the past few years, Graphene had attracted widely attention because of its excellent mechanical, thermal, electrical and optical properties (Brennan et al., 2017; Ilic et al., 2018; Solati and Dorranian, 2016; Tang et al., 2018; Wang et al., 2017). However, Graphene was a zero band-gap semiconductor with a symmetric band structure (Nayebi and Zaminpayma, 2017), which limited its application in the PEC biosensor. To our excitement, GDY, a new two-dimensional material, had been found and synthesized successfully. GDY was an allotrope of carbon which had the structure of highly π-conjugated (Jia et al., 2017). Up to now, GDY had been applied in many fields, for example, gas separation (Jiao et al., 2011), environmental cleaning (Gao et al., 2015), Li storage (Huang et al., 2015) and catalysis (Wang et al., 2011). Meanwhile, it was proved that GDY had a naturally band-gap, which was 0.47 eV calculated by density functional theory (Koo et al., 2014; Peng et al., 2014), indicating the application of photochemical was prospective. Some researchers had focused on the PEC performances of GDY (Li et al., 2016). However, to the best of our knowledge, the PEC biosensor based on GDY has not been reported.

In addition, to obtain strong photocurrent output was also a significant task, which determined the sensitivity of the assembled PEC platform. The PEC response could be improved by several ways, such as promoting charge separation or increasing the absorption of visible light of the semiconductor (Han et al., 2018; Ren et al., 2017a, 2017b; Shi et al., 2016; Wu et al., 2015; Yang et al., 2017). In this study, in order to improve the PEC performance of GDY, a photoactive material,

* Correspondence to: 53 Zhengzhou Road, Qingdao 266042, China.
E-mail address: hunxuprof@outlook.com (X. Hun).

https://doi.org/10.1016/j.bios.2019.02.002
Received 9 November 2018; Received in revised form 9 December 2018; Accepted 2 February 2019
Available online 04 February 2019
0956-5663/

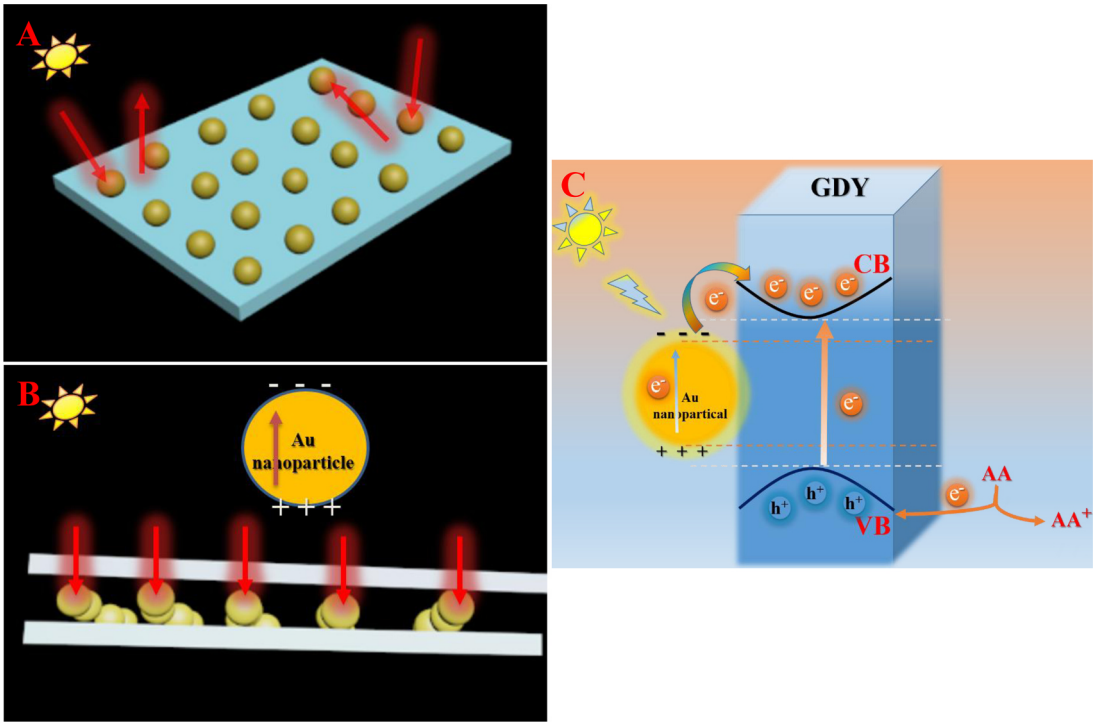

Scheme 1. The mechanism of the PEC response enhancement after loading AuNPs onto GDY. The AuNPs loaded on the surface of GDY (A). AuNPs combined with the GDY layers (B). The mechanism of PEC response of AuNPs-GDY in the presence of AA (C).

AuNPs-GDY, was successfully fabricated (Scheme 1). The AuNPs were grown on the GDY ingeniously and simply via a reduction reaction of chloroauric acid. The synthesized AuNPs-GDY utilized the tunable naturally band-gap of GDY and the surface plasmon resonance (SPR) effect of AuNPs which enhanced the absorption of visible light (Yang et al., 2017). The band-gap was tuned by loading AuNPs on GDY surface, which facilitate the charge carrier separation of GDY (Wu et al., 2015). Based on these two points, the PEC response of GDY was greatly improved. The relationship between the ratio of GDY to tetrachloroauric acid and the PEC response of AuNPs-GDY were studied intensively. AuNPs-GDY exhibited the best PEC response while the mass ratio of GDY to tetrachloroauric acid was 1:2.5.

A PEC biosensor based on AuNPs-GDY modified electrode was also fabricated. microRNA let-7a (let-7a), a significant disease marker, especially in the diagnosis of malignant tumors (Lu et al., 2005), was selected as a target. Due to its clinical significance, great efforts have been made for microRNA detection (Sun et al., 2018; Wang et al., 2018). The experimental results indicated that the synthesized photoactive material showed excellent PEC property and the developed PEC biosensor provided a highly efficient and sensitive miRNA assay.

2. Experimental section

2.1. Synthesis of AuNPs-GDY

The GDY was employed as the substrate material (GDY were kindly donated by Prof. Yuliang Li, Institute of Chemistry, Chinese Academy of Sciences, Beijing 100080, China). The synthetic method of GDY was shown in Supporting information (S 1.2). The AuNPs were deposited onto GDY by reduction of tetrachloroauric acid, applying sodium citrate as the reductant. Citrate reduction method was used to synthesize gold nanoparticles of different shapes and sizes by adding different masses of tetrachloroauric acid. The mass ratio of GDY to tetrachloroauric acid was 1:3.75, 1:2.5, 1:1.875, respectively. Typically, mixture solution of GDY and tetrachloroauric acid of different mass ratio were heated to 80 °C. Then a certain amount of sodium citrate solution was added to the solution rapidly under vigorous stirring. The product was collected after 30 min reaction. After washing three times with DMF, the product was placed in the brown bottle and stored at 4 °C for further use.

2.2. Characterization and detection

The morphology of pristine GDY and AuNPs-GDY was observed via FEI-Tecnai F20, 200 kV S/TEM. The bonding structure of pristine GDY and AuNPs-GDY was determined by Via-Reflex Raman spectroscopy. Then, to ascertain the particle size distribution of AuNPs on the GDY, ultraviolet absorption spectra was measured by Agilent Cary 100 UV–visible spectrophotometer. In order to characterize the electrochemical and PEC properties of AuNPs-GDY, various electrochemical measurements such as open circuit potential (OCP) and PEC performances were carried out on a CHI 660E electrochemical working station. PEC measurements were performed using a typical three-electrode configuration in which carbon paste electrode (CPE) or modified CPE was used as the working electrode, saturated calomel electrode as reference electrode and platinum wire as auxiliary electrode. A 10 W LED lamp was used as an irradiation source. Photocurrent was measured on a CHI 660E electrochemical working station.

3. Results and discussion

3.1. Morphology characterization of photoactive material

The TEM images of pristine GDY and AuNPs-GDY with different masses ratio were measured. As shown in Fig. 1**(A)**, the pristine GDY showed a lamellar structure with very thick layer, which provided a large area to load AuNPs. AuNPs-GDY with different masses ratio were shown in Fig. 1**(B)~(D)**. As we can see, the AuNPs were loaded on the surface and between the layers of GDY successfully. When the mass ratio of GDY to tetrachloroauric acid was 1:3.75, the AuNPs showed severe aggregation on GDY, and the shapes of the AuNPs were irregular (Fig. 1**(B)**). While the mass ratio turned to 1:2.5, the distribution of AuNPs was uniform and dispersed (Fig. 1**(C)**). But the shapes and the

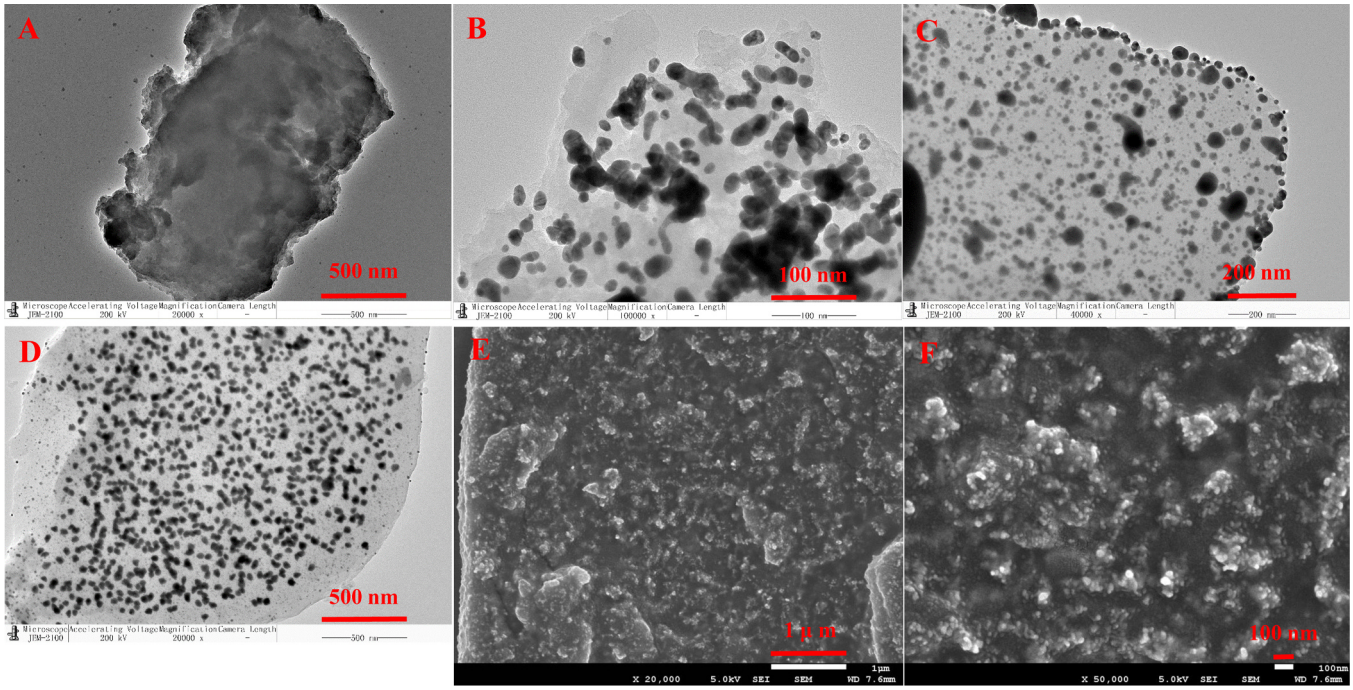

Fig. 1. TEM images of pristine GDY (A). TEM images of AuNPs-GDY compound with different masses ratio of GDY to tetrachloroauric acid: 1:3.75 (B); 1:2.5 (C); 1:1.875 (D). SEM images of AuNPs-GDY with the mass ratio of GDY to tetrachloroauric acid of 1:2.5 at different magnification (E, F).

particle size were still not uniform, and more AuNPs were inserted between the layers of GDY than that of the ratio of 1:3.75. If the mass ratio reduced to 1:1.875, AuNPs became regular and circular. There was no obvious agglomeration. And the vast majority of the AuNPs were loaded on the surface of GDY (Fig. 1**(D)**). Overall, with the decrease of the quality of tetrachloroauric acid, the distribution of AuNPs was gradually uniform and the shape of AuNPs was more regular. In order to further study the morphology of AuNPs-GDY, the SEM images were also measured at the mass ratio of 1:2.5. It could be clearly seen from Fig. 1**(E), (F)**, the AuNPs were loaded on the surface and between the layers of GDY successfully.

3.2. Optical and electrochemical properties of the photoactive material

In order to investigate the PEC properties of AuNPs-GDY, the amperometric i-t curve was measured using a typical three-electrode configuration (Detailed parameters was provided in the Supporting information). Herein, ascorbic acid (AA) was used as the electron donor for signal amplification. The concentration of AA was 10 μM. The results were displayed in Fig. 2**(A), (B)**. GDY modified CPE gave PEC signal about 101.7 nA (cure b), about 4.06 folds compared with that of the bare CPE (cure a). The main reason for the increase of the PEC signal was that the electrons of the photoelectrical active material undergone a transition under the excitation of light, generating electron-hole pairs, thereby producing the photocurrent (Link and El-Sayed, 1999). The experimental results indicated that GDY had optoelectronic activity. GDY produced photocurrent by generating the electron-hole pairs. When the AuNPs was loaded, the AuNPs-GDY modified CPE greatly enhanced PEC response. When the mass ratio of GDY to tetrachloroauric acid was 1:3.75 (cure c) the photocurrent was 534.6 nA which was 21.3 folds strengthened versus that of the bare CPE (cure a).

In addition, it was found that the mass ratio of GDY to tetrachloroauric acid changed, the photocurrent of AuNPs-GDY also changed accordingly. It was clear to see that the maximum photocurrent occurred at the mass ratio of GDY to tetrachloroauric acid was 1:2.5 (cure d), the photocurrent increased to around 789.0 nA, 31.43 folds than that of the bare CPE. The PEC response reduced to 487.9 nA at the mass ratio of 1:1.875 (cure e), 19.44 folds of that of the bare CPE. The results signified that after loading AuNPs, the GDY PEC responses were greatly improved. The results illustrated that the mass ratio of GDY to tetrachloroauric acid also played a key role in the enhancement of the PEC response. The trend of the mass ratios of GDY to tetrachloroauric acid and the PEC signal were shown in Fig. 2**(B)**. The folds of the PEC signal versus bare CPE were marked in red. When the mass ratio was 1:2.5, the PEC signal was the strongest. According to the TEM and the SEM images **(**Fig. 1**(C), (E) and (F))**, when the ratio was 1:2.5, the AuNPs loaded on the GDY were evenly distributed on the surface of the GDY and between the layers of GDY. Two reasons elucidated the enhancement of PEC response **(**Scheme 1**(A), (B))**. One was that the AuNPs loaded on the surface of GDY acted as scattering unit, which injected the light into the semiconductor layers, thereby increasing the capture rate of the visible light (Wu et al., 2013). The other was that AuNPs combined with the semiconductor layer, utilized the SPR effect of nanometer particles to inject more electrons into the semiconductor so that more electron hole pairs were produced and the recombination of the electron hole pairs was reduced (Pandikumar et al., 2010). The mechanism of PEC response of AuNPs-GDY was shown in Scheme 1**(C).** Under visible-light excitation, electrons on VB of GDY transited to CB forming electron-hole pairs, thereby generating the photocurrent. AuNPs loaded on the GDY generated electron-hole pairs due to the SPR effect, and the electrons of AuNPs flowed to the CB of GDY. Therefore, the AuNPs-GDY increased the output of the PEC signal. In addition, electron donor, AA, transferred electrons to the VB of GDY, thus enhancing the PEC output further. Hence, it showed that the SPR effect of the AuNPs played an important role in the PEC signal enhancement of the GDY.

Next, Raman spectroscopy was carried out to characterize the chemical bonding nature of pristine GDY and AuNPs-GDY and the SPR effect of AuNPs-GDY. As provided in Fig. 2**(C)**, the pristine GDY has two major peaks from 1275 cm^{-1} (A peak) to 1725 cm^{-1} (B peak). The A peak at 1479 cm^{-1} was due to the stretch of aromatic bonds which was similar to Graphene (Dresselhaus et al., 2010). The B peak at 1519 cm^{-1} came from vibrations of C-C bonds between triply coordinated atoms and their double coordinated neighbors (Tu et al.,

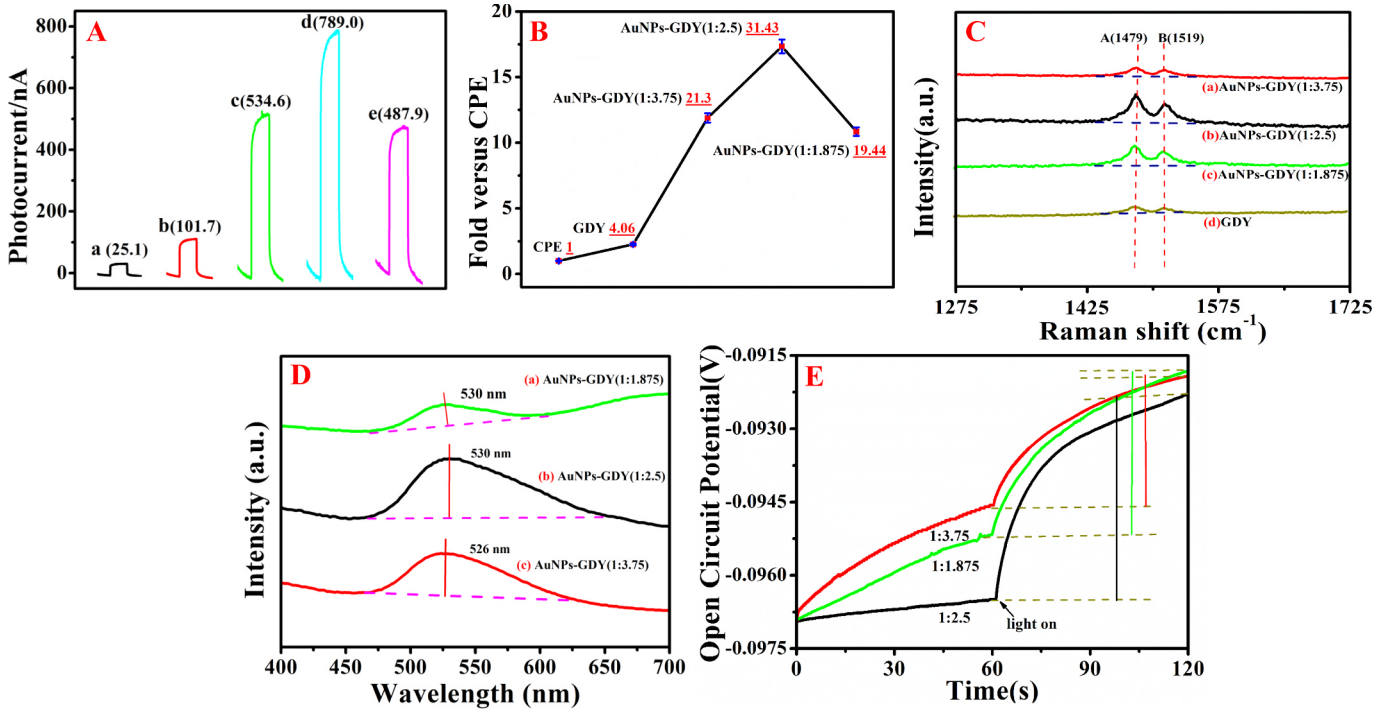

Fig. 2. (A) The PEC responses of bare CPE (a), GDY modified CPE (b), AuNPs-GDY modified CPE with mass ratio of GDY to tetrachloroauric acid of 1:3.75 (c), 1:2.5 (d), 1:1.875 (e). (B) The folds of PEC responses of different modified electrodes versus bare CPE. (C) The Raman spectroscopy of pristine GDY and AuNPs-GDY with different mass ratio of GDY to tetrachloroauric acid. (D) The ultraviolet spectroscopy of pristine GDY and AuNPs-GDY with different mass ratio of GDY to tetrachloroauric acid. (E) The open circuit potential AuNPs-GDY. The PEC and OCPT were carried out in pH 7.4 PBS contained 10 μM AA.

2016), which was only found in the Raman spectrum of GDY (cure d). It was well-known that AuNPs could enhance the Raman signal of other substances through the SPR effect of AuNPs (Lin et al., 2017; Suga et al., 2015). The Raman signals of AuNPs-GDY were all enhanced comparing with that of the pristine GDY. It indicated that AuNPs were loaded onto GDY successfully. These results were in accord with the TEM images. When the mass ratio of GDY to tetrachloroauric acid increased from 1:1.875 (cure c) to 1:2.5 (cure b), the Raman signals were enhanced. While, when the mass ratio increased to 1:3.75 (cure a), the Raman signal decreased instead. According to the reported work, noble metal nanoparticles enhance the Raman absorption of the substances by the SPR effect, which enhanced the surrounding magnetic field (Li et al., 2018a). As we all known the stronger SPR effect of the AuNPs, the stronger the Raman signal enhancement effect of the materials occurred (Shao et al., 2014). It demonstrated that when the mass ratio of GDY to tetrachloroauric acid was 1:2.5 (cure b), the SPR effect of AuNPs was the strongest, which was consistent with experimental phenomena of PEC measurement.

In order to confirm the SPR performance of the AuNPs-GDY further, the UV–vis was applied to characterize the light absorption of AuNPs-GDY (Fig. 2**(D)**). When the mass ratio of GDY to tetrachloroauric acid was 1:2.5, the maximum plasmon resonance enhanced absorption appeared at around 530 nm (cure b). It meant that AuNPs exhibited the strongest SPR effect in AuNPs-GDY when the mass ratio was 1:2.5. Furthermore, the location of the plasmon resonance peak occurred red shift (cure b) compared with that of the ratio of 1:3.75 (cure c), which indicated the increase of diameter of the AuNPs (Xie et al., 2010). It was proved that the SPR intensity became stronger with the increase of AuNPs size (Miao et al., 2015). The results suggested that when the mass ratio of GDY to tetrachloroauric acid was 1:2.5, the SPR effect of AuNPs was the strongest, which was in accord with the results of Raman spectroscopy.

Next, in order to ascertain that AuNPs inject electrons into the semiconductor, OCP test was measured under dark and illuminated conditions (Xiao et al., 2015). Under illumination, the OCP shifted to a more positive potential. It demonstrated that the electrons generated from the SPR effect of AuNPs injected to the hole of GDY. When the mass ratio was 1:2.5, the light exerted the highest potential shift (Fig. 2**(E)**). The experimental results showed that at the mass ratio of 1:2.5, the electrons injection from AuNPs to GDY was the most powerful (Chen et al., 2018). It further proved that when the mass ratio of GDY to tetrachloroauric acid was 1:2.5, the SPR effect of AuNPs was the strongest.

Through these experimental results and the theoretical analysis, it was found that the mass ratio of GDY to tetrachloroauric acid influence tremendously the SPR effect of AuNPs. The AuNPs which loaded on the surface and between layers of GDY produced SPR. Photocurrent increased with the increasing of mass ratio of GDY to tetrachloroauric acid. In addition, the biggest signal appeared at the mass ratio of GDY to tetrachloroauric acid was 1:2.5. Namely, when the mass ratio of GDY to tetrachloroauric acid was 1:2.5, the SPR effect of AuNPs was the strongest, which enhanced the PEC signal significantly.

3.3. Application of the photoactive material for PEC biosensor

Because AuNPs-GDY has eminent photoelectric activity, a PEC biosensor was established using AuNPs-GDY as photoactive material for practical application (Scheme 2). AuNPs-GDY was utilized as PEC substrate to modify the electrode. The capture RNA (cRNA) was immobilized onto AuNPs-GDY modified electrode. In the presence of target RNA, the probe RNA labeled with biotin hybridized with target RNA and formed a sandwich structure. After adding the streptavidin linked alkaline phosphatase (ALP), ALP bound with probe RNA (pRNA) and catalyzes the substrate, ascorbic acid 2-phosphate (AAP), to produce AA (Zhang et al., 2016). AA, the electron donors, was produced quantitatively, resulting in a significant PEC response. The sequences of let-7 family were shown in Table S1. The reason for employing ALP to generate AA was that ALP was captured on the electrode only when the target was present. It ensured that AA was generated due to the existence of the target. The blank was low because of no AA existing when

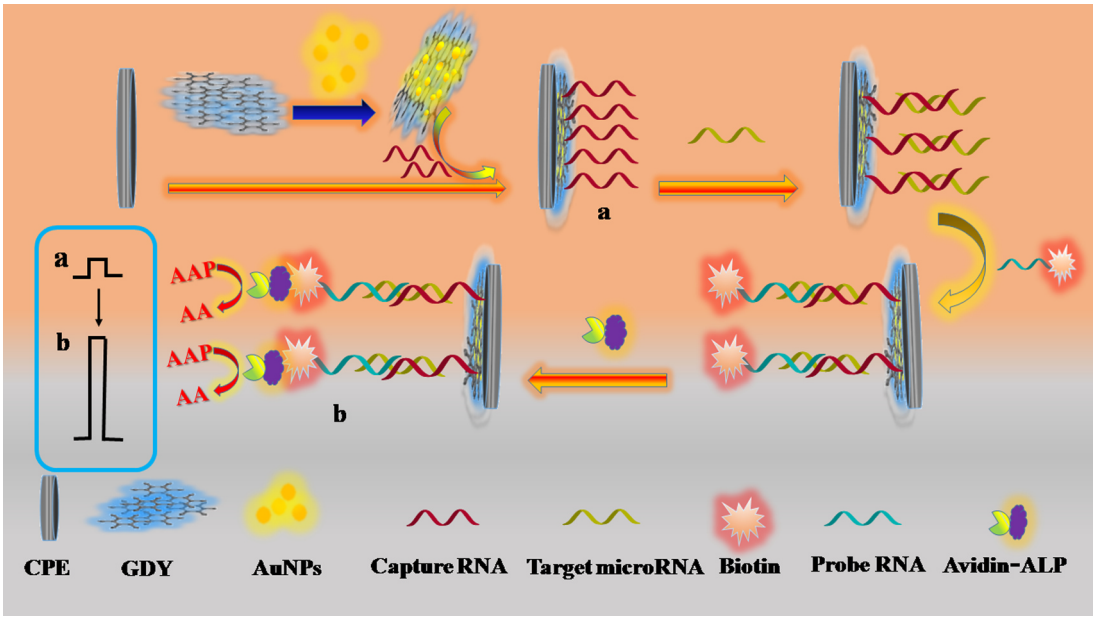

Scheme 2. Schematic illustration of PEC biosensor based on AuNPs-GDY modified electrode for let-7a microRNA detection.

these were no target (Detailed information can be seen in the Section 3.4).

3.4. PEC properties, fabrication process characterization, detection performance and practical sample detection of biosensor

When the ratio of GDY to tetrachloroauric acid was 1:2.5 AuNPs-GDY exhibited the most remarkable PEC response, so it was used to modify electrode. The PEC responses of bare CPE, AuNPs-GDY modified CPE and modified CPE incubated with the mixture of cRNA, let-7a, pRNA and the streptavidin linked ALP were measured. As shown in Fig. 3**(A)**, the bare CPE presented only 1.2 nA, almost no PEC response (cure a). The AuNPs-GDY modified CPE give about 29.6 nA (cure b), which had a certain improvement compared with that of the bare CPE. Then, after incubated with the mixture of cRNA, let-7a, biotin labeled pRNA and the streptavidin linked alkaline phosphatase, the PEC response of the modified CPE came up to almost 416.3 nA (cure c), 14.1 folds as much as that of the AuNPs-GDY modified CPE.

To further characterize the construction process of PEC biosensor step by step, the EIS measurements were performed in 5.0 mM $[Fe(CN)_6]^{3-/4-}$ solution at potential of 0.23 V. Numerical values of Ret were derived from experimental impedance spectra by fitting an equivalent circuit model based on a modified Randles model to the data. As shown in Fig. 3**(B)**, Ret, the charge-transfer resistance, of bare CPE was 120 Ω (curve a). When GDY was modified onto CPE, Ret was 450 Ω which increased obviously comparing with bare CPE (curve b). The Ret increased because of the poor conductivity of GDY. However, when the surface of the electrode was modified with AuNPs-GDY, the Ret decreased sharply to 95 Ω (curve c). This was caused by the good electrical conductivity of AuNPs. After immobilization of cRNA, the Ret increased afresh to 800 Ω (curve d). It was due to the phosphate groups of RNA produced a negatively charged layer, that reduced the ability of $[Fe(CN)_6]^{3-/4-}$ approaching the surface of electrode and the lower conductivity of cRNA. After electrode was blocked by MCH, the Ret increased furtherly to 950 Ω (curve e). When let-7a, pRNA and streptavidin linked alkaline phosphatase were added, the Ret increased continuously to 1700 Ω (curve f), which was attributed to the lower electron-transfer abilities of the RNA, and the augment of steric

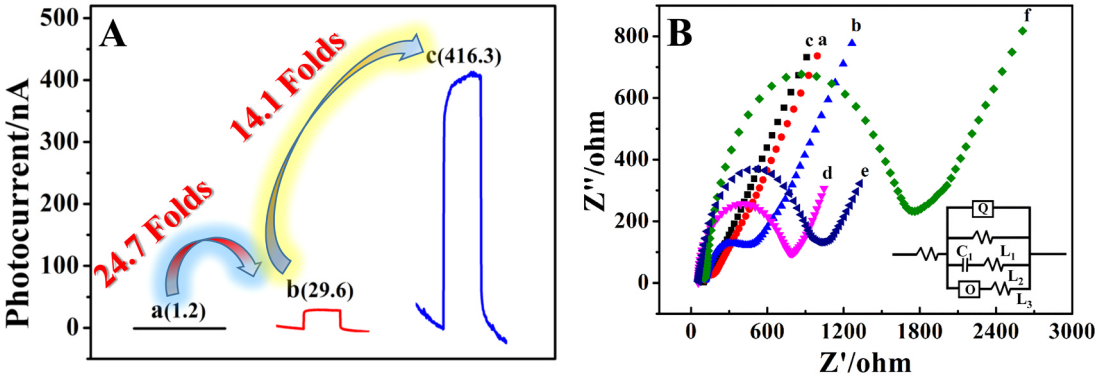

Fig. 3. (A) The PEC responses of different working electrode. Bare CPE (a); AuNPs-GDY modified CPE at the mass ratio of 1:2.5 (b); AuNPs-GDY modified CPE incubated with the mixture of cRNA, let-7a, pRNA and the streptavidin linked alkaline phosphatase (c). The concentration of let-7a was 100 pM. The PEC detection was carried out in 0.1 M pH 7.4 PBS contained 10 mM AAP. (B) Nyquist plot of different working electrode in 0.1 M KCl solution contained 5.0 mM $K_3Fe(CN)_6/K_4Fe(CN)_6$. a: Bare CPE; b: GDY modified CPE; c: AuNPs-GDY modified CPE; d: cRNA/AuNPs-GDY modified CPE; e: cRNA/MCH/AuNPs-GDY modified CPE (e); f: pRNA/cRNA/MCH/AuNPs-GDY modified CPE in the presence of 100 pM tRNA.

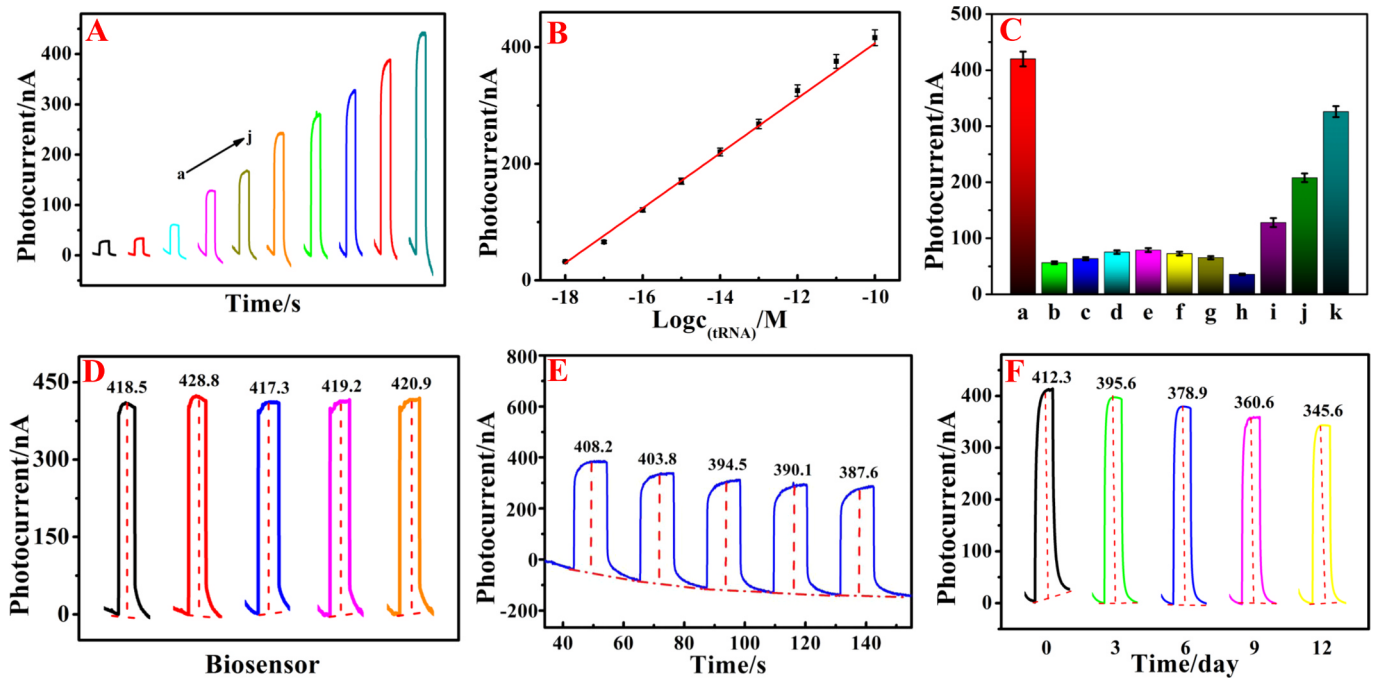

Fig. 4. (A) PEC responses of the PEC biosensor toward different concentrations of let -7a. From a to j: 0, 0.001, 0.01, 0.1, 1, 10, 100, 1000, 10000, 100000 fM. (B) The linear relationship of the PEC responses to the logarithm of let-7a concentration. (C) Selectivity and specificity of the designed PEC biosensor. a to h: let-7a, let-7b, let-7c, let-7d, let-7e, let-7 f, let-7g (The concentrations of let-7a and six other let-7 microRNA family were 100 pM and 10 nM, respectively); h: blank; i: 100 fM let-7a; j: serum sample; k: mixture of 100 fM let-7a and human serum, respectively. (D) Reproducibility of designed PEC biosensor. Five biosensors were tested in parallel. (E) Time-based photocurrent responses of the PEC biosensor. (F) Stability of designed PEC biosensor for 12 days storage: 0st, 3rd, 6th, 9th, 12th. The concentration of let-7a was 100 pM in 0.1 M pH 8.0 PBS contained 10 mM AAP.

hindrance. The distinct varying of Ret indicated the successful construction of the PEC biosensor.

After the optimization of experimental conditions (S 2.1), the detection performance, selectivity, reproducibility and stability of the fabricated PEC biosensor were investigated (Detailed processes were provided in the Supporting information as S 2.2 and S 2.3). The linear range of this PEC biosensor was from 1.0×10^{-18} M to 1.0×10^{-10} M with the detection limit of 3.3×10^{-19} M (LOD = 3 S/N) (Fig. 4**(A), (B))**. It had wide-range linear and low detection limit comparing with other PEC methods (Table S2). This method had high sensitivity due to the following reasons. Firstly, ALP specifically catalyzed AAP to generate AA in situ for sacrificial electron donating. It provided a low background signal. Secondly, high catalytic efficiency of ALP coupled with high PEC properties of AuNPs-GDY produced strong PEC response. To verify the selectivity of the PEC sensor, other six let-7 family microRNA were inspected. As shown in Fig. 4(C), no significant change in the PEC response was noticed in the presence of the nontarget substances. The specificity of PEC biosensor was also detected in human serum samples. The signal of the PEC biosensor with the mixture solution (100 pM let-7a was added into serum sample) exhibited a sum signal of PEC signal from pure let-7a (100 fM) and serum sample let-7a (68 fM). The results suggested this biosensor has good selectivity and specificity.

The reproducibility of the PEC biosensor was evaluated by analyzing five independently prepared biosensors. The coefficients of variation between assays were 4.5% (Fig. 4**(D)**). The stability was investigated by five successive determinations or measuring every 3 days storing the biosensor at 4 °C (Fig. 4**(E), (F)**). After 12 days storage, no significant change was found in PEC response and the PEC response was 83.8% of its initial response to 100 pM let-7a (Fig. 4**(F))**. And the PEC biosensor still retained 95.0% initial response ability after five repeated detection (Fig. 4**(E))**. The results illustrated that this biosensor exhibited satisfactory stability. Then, the application of the fabricated PEC biosensor in complex biological matrixes was also carried out (S 2.4). To estimate the application of this PEC biosensor, three healthy person serum samples and three Renal clear cell carcinoma (ccRCC) patients serum samples were detected. As presented in Table S2 the concentrations of let-7a were 0.064, 0.058, 0.069 pM in healthy human serum samples and the concentrations of let-7a were 0.021, 0.035, 0.027 pM in ccRCC patients serum samples. It signified that the concentration of let-7a in plasma of patients with malignant tumors was obviously lower than that of normal people. The results were consistent with the literature description (Sun et al., 2013). The recoveries were within 96.2%, to 101.1%. The results indicated that the PEC biosensor showed acceptable accuracy and reliability towards microRNA detection in the human serum samples (Table S2).

4. Conclusions

Overall, an innovative photoactive material, AuNPs-GDY, was synthesized successfully. The AuNPs were deposited onto GDY by reduction of tetrachloroauric acid, applying sodium citrate as the reductant. The SPR effect caused by the AuNPs, which grown on the surface and between the layers of GDY, played a key role in enhancing PEC signal. The mass ratio of GDY to tetrachloroauric acid effected SPR and PEC response greatly. When the mass ratio was 1:2.5, the SPR effect of AuNPs was strongest, resulting in the highest PEC response. Based on this discovery, a PEC biosensor was constructed based on AuNPs-GDY modified electrode. Moreover, this PEC biosensor showed prominent reliability, excellent selectivity and good stability for the let-7a microRNA detection. This PEC biosensor exhibited a great potential for application in microRNA detection in the human serum samples and open a new prospect of let-7a detection.

CRediT authorship contribution statement

Yanxin Li: Data curation, Formal analysis, Investigation, Methodology, Visualization, Writing - original draft, Writing - review & editing. **Xiaohua Li:** Conceptualization, Investigation, Writing - review & editing. **Yuchan Meng:** Data curation, Formal analysis, Investigation, Methodology, Writing - original draft, Writing - review & editing. **Xu Hun:** Conceptualization, Data curation, Formal analysis, Funding acquisition, Investigation, Methodology, Project administration, Resources, Software, Supervision, Validation, Visualization, Writing - original draft, Writing - review & editing.

Acknowledgements

This work was supported by National Natural Science Foundation of China (21575073), Applied Basic Research Plan Project of Datong City, China (2018158) and Laoshan Scholar Program of Qingdao University of Science and Technology (201802685).

Declaration of interests

None.

Appendix A. Supporting information

Supplementary data associated with this article can be found in the online version at doi:10.1016/j.bios.2019.02.002.

References

Brennan, B., Spencer, S.J., Belsey, N.A., Faris, T., Cronin, H., Silva, S.R.P., Sainsbury, T., Gilmore, I.S., Stoeva, Z., Pollard, A.J., 2017. Structural, chemical and electrical characterisation of conductive graphene-polymer composite films. Appl. Surf. Sci. 403, 403–412.

Chen, Y.-C., Hsu, Y.-K., Popescu, R., Gerthsen, D., Lin, Y.-G., Feldmann, C., 2018. Au@Nb@HxK1-xNbO$_3$ nanopeapods with near-infrared active plasmonic hot-electron injection for water splitting. Nat. Commun. 9 (1), 232.

Dresselhaus, M.S., Jorio, A., Hofmann, M., Dresselhaus, G., Saito, R., 2010. Perspectives on Carbon Nanotubes and Graphene Raman Spectroscopy. Nano Lett. 10 (3), 751–758.

Fan, D., Bao, C., Khan, M.S., Wang, C., Zhang, Y., Liu, Q., Zhang, X., Wei, Q., 2018a. A novel label-free photoelectrochemical sensor based on N,S-GQDs and CdS co-sensitized hierarchical Zn_2SnO_4 cube for detection of cardiac troponin I. Biosens. Bioelectron. 106, 14–20.

Fan, D., Bao, C., Liu, X., Wu, D., Zhang, Y., Wang, H., Du, B., Wei, Q., 2018b. A novel label-free photoelectrochemical immunosensor based on NCQDs and Bi_2S_3 co-sensitized hierarchical mesoporous SnO2 microflowers for detection of NT-proBNP. J. Mater. Chem. B 6 (46), 7634–7642.

Gao, X., Zhou, J., Du, R., Xie, Z., Deng, S., Liu, R., Liu, Z., Zhang, J., 2015. Robust superhydrophobic foam: a graphdiyne-based hierarchical architecture for oil/water separation. Adv. Mater. 28 (1), 168–173.

Han, Q., Wang, R., Xing, B., Chi, H., Wu, D., Wei, Q., 2018. Label-free photoelectrochemical aptasensor for tetracycline detection based on cerium doped CdS sensitized $BiYWO_6$. Biosens. Bioelectron. 106, 7–13.

Huang, C., Zhang, S., Liu, H., Li, Y., Cui, G., Li, Y., 2015. Graphdiyne for high capacity and long-life lithium storage. Nano Energy 11, 481–489.

Ilic, O., Thomas, N., Christensen, T., Sherrott, M., Soljačić, M., Minnich, A., Miller, O., Atwater, H., 2018. Active radiative thermal switching with graphene plasmon resonators. ACS Nano 12 (3), 2474–2481.

Jia, Z., Li, Y., Zuo, Z., Liu, H., Huang, C., Li, Y., 2017. Synthesis and properties of 2D carbon—graphdiyne. Acc. Chem. Res. 50 (10), 2470–2478.

Jiao, Y., Du, A., Hankel, M., Zhu, Z., Rudolph, V., Smith, S.C., 2011. Graphdiyne: a versatile nanomaterial for electronics and hydrogen purification. Chem. Commun. 47 (43), 11843–11845.

Koo, J., Park, M., Hwang, S., Huang, B., Jang, B., Kwon, Y., Lee, H., 2014. Widely tunable band gaps of graphdiyne: an ab initio study. Phys. Chem. Chem. Phys. 16 (19), 8935–8939.

Li, J., Gao, X., Liu, B., Feng, Q., Li, X.-B., Huang, M.-Y., Liu, Z., Zhang, J., Tung, C.-H., Wu, L.-Z., 2016. Graphdiyne: a metal-free material as hole transfer layer to fabricate quantum dot-sensitized photocathodes for hydrogen production. J. Am. Chem. Soc. 138 (12), 3954–3957.

Li, J., Pei, Q., Wang, R., Zhou, Y., Zhang, Z., Cao, Q., Wang, D., Mi, W., Du, Y., 2018a. Enhanced photocatalytic performance through magnetic field boosting carrier transport. ACS Nano 12 (4), 3351–3359.

Li, Z., Zhang, J., Li, Y., Zhao, S., Zhang, P., Zhang, Y., Bi, J., Liu, G., Yue, Z., 2018b. Carbon dots based photoelectrochemical sensors for ultrasensitive detection of glutathione and its applications in probing of myocardial infarction. Biosens. Bioelectron. 99, 251–258.

Lin, D., Wu, Z., Li, S., Zhao, W., Ma, C., Wang, J., Jiang, Z., Zhong, Z., Zheng, Y., Yang, X., 2017. Large-area Au-nanoparticle-functionalized Si nanorod arrays for spatially uniform surface-enhanced Raman spectroscopy. ACS Nano 11 (2), 1478–1487.

Link, S., El-Sayed, M.A., 1999. Size and temperature dependence of the plasmon absorption of colloidal gold nanoparticles. J. Phys. Chem. B 103 (21), 4212–4217.

Lu, J., Getz, G., Miska, E.A., Alvarez-Saavedra, E., Lamb, J., Peck, D., Sweet-Cordero, A., Ebert, B.L., Mak, R.H., Ferrando, A.A., Downing, J.R., Jacks, T., Horvitz, H.R., Golub, T.R., 2005. MicroRNA expression profiles classify human cancers. Nature 435, 834.

Miao, J., Hu, W., Jing, Y., Luo, W., Liao, L., Pan, A., Wu, S., Cheng, J., Chen, X., Lu, W., 2015. Surface plasmon-enhanced photodetection in few layer MoS_2 phototransistors with Au nanostructure arrays. Small 11 (20), 2392–2398.

Nayebi, P., Zaminpayma, E., 2017. Metal decorated graphdiyne: a first principle study. Phys. B: Condens. Matter 521, 112–121.

Pandikumar, A., Murugesan, S., Ramaraj, R., 2010. Functionalized silicate sol–gel-supported TiO_2–Au core–shell nanomaterials and their photoelectrocatalytic activity. ACS Appl. Mater. Interfaces 2 (7), 1912–1917.

Peng, G., Hongye, B., Chunfa, L., Yilin, G., Dongbo, X., Biyi, C., Teng, X., Weiqiang, F., Weidong, S., 2018. Integrated heterostructure of PDA/Bi-AgIn5S_8/TiO_2 for photoelectrochemical hydrogen production: understanding the synergistic effect of multilayer structure. Adv. Mater. Interfaces 5 (10), 1701574.

Peng, Q., Dearden, A.K., Crean, J., Han, L., Liu, S., Wen, X., De, S., 2014. New materials graphyne, graphdiyne, graphone, and graphane: review of properties, synthesis, and application in nanotechnology. Nanotechnol. Sci. Appl. 1–29.

Ren, X., Ma, H., Zhang, T., Zhang, Y., Yan, T., Du, B., Wei, Q., 2017a. Sulfur-doped graphene-based immunological biosensing platform for multianalysis of cancer biomarkers. ACS Appl. Mater. Interfaces 9 (43), 37637–37644.

Ren, X., Zhang, T., Wu, D., Yan, T., Pang, X., Du, B., Lou, W., Wei, Q., 2017b. Increased electrocatalyzed performance through high content potassium doped graphene matrix and aptamer tri infinite amplification labels strategy: highly sensitive for matrix metalloproteinases-2 detection. Biosens. Bioelectron. 94, 694–700.

Shao, J., Li, W., Zhou, X., Hu, J., 2014. Magnetic-field-assisted hydrothermal synthesis of 2 × 2 tunnels of MnO2 nanostructures with enhanced supercapacitor performance. CrystEngComm 16 (43), 9987–9991.

Shi, X.-M., Fan, G.-C., Shen, Q., Zhu, J.-J., 2016. Photoelectrochemical DNA biosensor based on dual-signal amplification strategy integrating inorganic–organic nanocomposites sensitization with λ-exonuclease-assisted target recycling. ACS Appl. Mater. Interfaces 8 (51), 35091–35098.

Solati, E., Dorranian, D., 2016. Nonlinear optical properties of the mixture of ZnO nanoparticles and graphene nanosheets. Appl. Phys. B 122 (4), 76.

Suga, K., Yoshida, T., Ishii, H., Okamoto, Y., Nagao, D., Konno, M., Umakoshi, H., 2015. Membrane Surface-Enhanced Raman Spectroscopy (MSERS) for Sensitive Detection of Molecular Behaviour of Lipid Assemblies.

Sun, X., Qin, S., Fan, C., Xu, C., Du, N., Ren, H., 2013. Let-7: a regulator of the ERα signaling pathway in human breast tumors and breast cancer stem cells. Oncol. Rep. 29 (5), 2079–2087.

Sun, X., Wang, H., Jian, Y., Lan, F., Zhang, L., Liu, H., Ge, S., Yu, J., 2018. Ultrasensitive microfluidic paper-based electrochemical/visual biosensor based on spherical-like cerium dioxide catalyst for miR-21 detection. Biosens. Bioelectron. 105, 218–225.

Tang, Q., Zhen, T., Danyun, L.I., Gao, Q., 2018. Mechanical properties of graphene/hydroxyapatite composite materials: numerical study. Chin. J. Comput. Phys. 1, 15–17.

Tu, W., Cao, H., Zhang, L., Bao, J., Liu, X., Dai, Z., 2016. Dual signal amplification using gold nanoparticles-enhanced zinc selenide nanoflakes and P19 protein for ultrasensitive photoelectrochemical biosensing of microRNA in cell. Anal. Chem. 88 (21), 10459–10465.

Wang, H., Jian, Y., Kong, Q., Liu, H., Lan, F., Liang, L., Ge, S., Yu, J., 2018. Ultrasensitive electrochemical paper-based biosensor for microRNA via strand displacement reaction and metal-organic frameworks. Sens. Actuators B: Chem. 257, 561–569.

Wang, S., Yi, L., Halpert, J.E., Lai, X., Liu, Y., Cao, H., Yu, R., Wang, D., Li, Y., 2011. A novel and highly efficient photocatalyst based on P25–graphdiyne nanocomposite. Small 8 (2), 265–271.

Wang, X., Xu, R., Sun, X., Wang, Y., Ren, X., Du, B., Wu, D., Wei, Q., 2017. Using reduced graphene oxide-Ca: cdse nanocomposite to enhance photoelectrochemical activity of gold nanoparticles functionalized tungsten oxide for highly sensitive prostate specific antigen detection. Biosens. Bioelectron. 96, 239–245.

Wu, D., Yan, K., Zhou, Y., Wang, H., Lin, L., Peng, H., Liu, Z., 2013. Plasmon-enhanced photothermoelectric conversion in chemical vapor deposited graphene p–n junctions. J. Am. Chem. Soc. 135 (30), 10926–10929.

Wu, G., Li, P., Xu, D., Luo, B., Hong, Y., Shi, W., Liu, C., 2015. Hydrothermal synthesis and visible-light-driven photocatalytic degradation for tetracycline of Mn-doped $SrTiO_3$ nanocubes. Appl. Surf. Sci. 333, 39–47.

Xiao, J., Shi, J., Liu, H., Xu, Y., Lv, S., Luo, Y., Li, D., Meng, Q., Li, Y., 2015. Efficient $CH_3NH_3PbI_3$ perovskite solar cells based on graphdiyne (GD)-modified P3HT hole-transporting material. Adv. Energy Mater. 5 (8), 1401943.

Xie, X.N., Zhong, Y.L., Dhoni, M.S., Xie, Y., Loh, K.P., Sow, C.H., Ji, W., Wee, A.T.S., 2010. UV–visible-near infrared photoabsorption and photodetection using close-packed metallic gold nanoparticle network. J. Appl. Phys. 107 (5), 053510.

Yang, H., Zhang, Y., Zhang, L., Cui, K., Ge, S., Huang, J., Yu, J., 2018. Stackable lab-on-paper device with all-in-one Au electrode for high-efficiency photoelectrochemical cyto-sensing. Anal. Chem. 90 (12), 7212–7220.

Yang, K., Zhang, Y., Meng, C., Cao, F., Chen, X., Fu, X., Dai, W., Yu, C., 2017. Well-crystallized $ZnCo_2O_4$ nanosheets as a new-style support of Au catalyst for high efficient CO preferential oxidation in H2 stream under visible light irradiation. Appl. Surf. Sci. 391, 635–644.

Zhang, N., Ma, Z.-Y., Ruan, Y.-F., Zhao, W.-W., Xu, J.-J., Chen, H.-Y., 2016. Simultaneous photoelectrochemical immunoassay of dual cardiac markers using specific enzyme tags: a proof of principle for multiplexed bioanalysis. Anal. Chem. 88 (4), 1990–1994.

Zhao, W.W., Xu, J.J., Chen, H.Y., 2014. Photoelectrochemical DNA biosensors. Chem. Rev. 114 (15), 7421–7441.